

The Optical Alignment System of the ZEUS MicroVertex Detector

K. Korcsak-Gorzo, G. Grzelak,¹ K. Oliver, M. Dawson,
R. Devenish,^{*} J. Ferrando, T. Matsushita,² P. Shield,³
R. Walczak

*Department of Physics, University of Oxford,
Denys Wilkinson Building, Keble Road, Oxford OX1 3RH*

Abstract

The laser alignment system of the ZEUS microvertex detector is described. The detector was installed in 2001 as part of an upgrade programme in preparation for the second phase of electron-proton physics at the HERA collider. The alignment system monitors the position of the vertex detector support structure with respect to the central tracking detector using semi-transparent amorphous-silicon sensors and diode lasers. The system is fully integrated into the general environmental monitoring of the ZEUS detector and data has been collected over a period of 5 years. The primary aim of defining periods of stability for track-based alignment has been achieved and the system is able to measure movements of the support structure to a precision around $10\ \mu\text{m}$.

Key words: Alignment, vertex detector, laser, semi-transparent sensors.

1 Introduction

A silicon-strip MicroVertex Detector (MVD) was added to the ZEUS detector in 2001 as part of an upgrade programme for high luminosity running with the HERA-II electron-proton collider at DESY[1]. One of the main physics motivations was to improve the study of heavy flavour production at HERA, particularly charm. With mean decay lengths of the order of $100\ \mu\text{m}$ for charmed

^{*} Corresponding author. Email: r.devenish@physics.ox.ac.uk

¹ Now at the University of Warsaw.

² Now at Imperial College, London.

³ Retired.

hadrons, precise alignment of the MVD active elements is crucial if their intrinsic spatial resolution of $10\ \mu\text{m}$ and better is to be properly exploited. Alignment has been addressed in three stages: i) during construction the position of the silicon strip detectors was measured with respect to the local support structure using an accurate 3-D measuring machine; ii) an optical alignment system tracks large movements of the MVD support structure; iii) individual MVD sensors are aligned precisely using charged-particle tracks from HERA run data. This paper describes the laser alignment system used for the second stage and summarises its performance. The primary aims of the laser system are to track large movements (at the level of $100\ \mu\text{m}$) of the MVD support structure with respect to the central tracking detector (CTD) and to define periods of stability for the track alignment. A prototype [2] of the system described here was tested and used during the construction of the MVD.

The paper is organised as follows: the MVD is described very briefly in the next section; the optical alignment system is described in section 3; the read-out and online control system is described in section 4; data reduction and reconstruction is covered in section 5; the results are summarised in section 6 and the paper concludes with a short summary (section 7).

2 The ZEUS Microvertex Detector

The space available for the MVD is limited by the CTD and the shape of the beam pipe. The space inside the tracking detector has a length of about 2 m and a diameter of 32 cm. The design requirements of the MVD were: polar angular coverage of $10^\circ - 170^\circ$; at least three measurements, in two projections, per track; at least $20\ \mu\text{m}$ hit resolution and impact parameter resolution of around $100\ \mu\text{m}$ at 90° for tracks with momentum of at least $2\ \text{GeV}/c$. In order to meet these requirements within the limited space, the MVD consists of two parts, barrel and wheels, which are supported by a carbon-fibre tube made in two half-cylinders. The barrel has three concentric layers of silicon sensors but only the forward region is instrumented with sensors mounted on four wheels, numbered from 0 to 3. This follows from the unequal HERA beam energies, with 27.5 GeV electrons and 920 GeV protons, reaction products are boosted along the forward proton direction. The layout of the MVD is shown in Fig. 1 and Fig. 2 shows cross sections of the barrel and a wheel. All the MVD services and readout connections are made through the rear end of the detector. The region at the rear of the MVD (shown to the right of the barrel in Fig. 1) is used for cooling water distribution manifolds. The MVD is described in more detail in references [3] and [4]. As the MVD has to fit into an existing detector, getting services in and out is not easy. The route that cables follow is close to the rear beampipe, through the beam hole in the rear tracking detector and rear calorimeter. A further challenge is that, as part

of the measures to increase the luminosity for HERA-II, a superconducting combined-function magnet (the HERA GG magnet) penetrates the detector around the rear beampipe. Getting all the MVD cables to fit between this magnet and the rear calorimeter was particularly challenging. The special very thin cables designed to keep material at a minimum within the detector run for about five metres from the MVD to four cable patch-boxes located above the first HERA magnets outside the ZEUS detector on the rear (upstream proton) side. From here much more robust cables take services and signals to the MVD services and readout racks about 20 m away.

3 Optical Alignment System

The MVD laser alignment system consists of five straightness monitors placed around the circumference of the MVD support tube. Each straightness monitor consists of a collimated laser beam, approximately parallel to the collider beam line, with seven semi-transparent silicon sensors positioned along its path. Two of the sensors, mounted on the forward and rear CTD end-plates, define the line for that laser beam. The five remaining sensors are mounted within the MVD at the forward and rear end-flanges, the forward and rear barrel-flanges and the support structure for wheel-3, as shown schematically in Fig. 3. Inside the MVD a laser beam is contained between sensors within a narrow carbon-fibre cover with a semicircular profile, glued to the inner surface of the outer half-cylinders. Each sensor provides two mutually orthogonal position measurements, with resolution better than $10\ \mu\text{m}$, in a local sensor coordinate system. The alignment system is sensitive to rotations, twists and sags of the MVD support structure with respect to the CTD from which it is mounted. The system is not sensitive to translations along the beam direction.

3.1 Position sensors and signal cables

The laser position sensors, DPSD-516 transparent silicon diodes (TSD), use semi-transparent amorphous-silicon as the active material. The sensors were developed by H. Kroha *et. al.* [5] and manufactured by EG&G Heimann Opto-electronics. The active material of the TSD sensors has a thickness of $\sim 1\ \mu\text{m}$ and an area of $5 \times 5\ \text{mm}^2$. Signals are read out by strips made of $\sim 100\ \text{nm}$ thick indium-tin-oxide, with 16 strips on each side of the amorphous-silicon. The strips on opposite sides are perpendicular to each other, with strip pitch $312\ \mu\text{m}$ and strip gap $10\ \mu\text{m}$. The whole structure is deposited on a $0.5\ \text{mm}$ thick glass substrate. The sensor is transparent to light with wavelength greater than $\sim 600\ \text{nm}$. Transmission reaches a rough plateau of 80% at wavelengths around $700\ \text{nm}$ and above, as shown in Fig. 6 of reference [2]. However

the sensitivity of the sensor drops fairly rapidly above 700 nm. Full details of the sensor and its performance are given in reference [5].

Sensors are positioned in planes perpendicular to the beamline at seven locations:⁴ 0 (RCTD) and 7 (FCTD) are attached to the CTD at its rear and forward end-plates, respectively; 1 (RMVD) and 6 (FMVD) are just inside the rear and forward end flanges of the MVD support tube, respectively; 2 (RBarrel) and 3 (FBarrel) are on the rear and forward MVD barrel-flanges and 5 (Wheel-3) is at the position of MVD most forward wheel, wheel-3. Plane-4 at the position of wheel-1 could not be installed because of space constraints. The TSD sensor strip signals are read out in a local $x - y$ coordinate system where x is defined to be from the bottom ohmic contacts (cathodes) and y from the upper bias voltage contacts (anodes). For space reasons the sensors on the two planes at the rear end had to be mounted in a reversed orientation. Fig. 4 shows the orientation of the local coordinate systems for standard and reversed sensors (top figures). The bottom figure shows the bonding of the special flat readout cable to sensor strips in the standard mounting. Note that the coordinate will vary in a direction at right-angles to the readout strips.

The relationship between the sensor local coordinate system and the ZEUS coordinate system depends on the sensor location. More details are given in the section on reconstruction and data analysis. The readout cables for the sensors presented quite a challenge. Although the MVD has a much higher spatial precision than the large drift chamber outside it, the benefit of these points could be significantly reduced in the overall track fit if the MVD increased the multiple scattering by too much. Thus the readout cables had to have minimum mass and, as there was no space for on- or near-detector amplification, the impedance of the cables over the total length from sensor to readout board of around 25 m had to be kept low. A special cable was designed and fabricated by Oxford engineers and technical staff. Using a photo-fabrication technique $32 \times 250 \mu\text{m}$ tracks were etched onto a $1 \text{ m} \times 0.5 \text{ m}$ flexible kapton-backed copper sheet. Then using an ingenious ‘cut and fold’ technique continuous flexible cables with thickness of only $200 \mu\text{m}$ and of various lengths up to 20 m were produced.

3.2 Lasers and optical fibres

The wavelength of the laser should be long enough to give good sensor transmission, but short enough to have adequate sensor sensitivity. The available aperture for the laser beam is $5 \times 5 \text{ mm}^2$ and the beam should be contained in the aperture over a length of 2 m. Taking all these requirements into consideration, the laser was chosen to have a wavelength of 780 nm, a gaussian

⁴ Table 1 gives the precise positions.

profile and a beam diameter of 1.5 mm at the waist. More details on the characterisation of the laser beam are given in reference [2]. The positions of the five laser beams around the circumference of the MVD support tube are shown in Fig. 5. A sixth laser beam was planned at the position 208.25° but had to be abandoned because of conflicting demands for space. The numbering and power of the lasers are given in Table 2. Unfortunately beam-0 was knocked out of alignment during work to modify a radiation absorber inside the beampipe at the rear end of the MVD. Given the extreme difficulty of reaching the optical fibre laser heads at this time, the beam could not be re-aligned. The lasers, IFLEX600 CW with maximum power rating of 5.2 mW and 0.65 mm collimated output, were provided by Point Source [6]. The lasers and their power supplies are positioned with other MVD service and readout crates about 25 m from the detector. The laser beams are carried by optical fibres,⁵ following the cable route through the patch box, with fibre connectors, to the laser fibre heads at the rear end of the MVD support tube. The fibre heads are mounted on a ring attached to the CTD and ‘pointing’ adjustments for a laser beam are made using three screws for each head. Given the very limited space between the beam pipe and the CTD rear on-board electronics, the final adjustment is a difficult and delicate task, that becomes impossible once the rear tracking detector is installed.

The lasers and their power supplies are contained in two ‘shutter boxes’, one box with three lasers and the other box with two lasers. Once the lasers are powered on, the light output can be ‘switched’ on or off by opening or closing a mechanical shutter across all three laser beams. The shutter is moved by an electromagnet which can be under operator or software control. The shutter control is also interfaced to the ZEUS slow-control and safety interlock systems. In normal operation the lasers are powered continuously to avoid fluctuations when they are powered up. The beams are switched on or off for the various data collection procedures by use of the shutters.

3.3 Sensor Resolution

Before installation the TSD sensors were characterised using a test set-up consisting of a computer controlled two-dimensional translation stage mounted on an optical rail system [2]. For a given sensor plane the basic measurements are strip signals above the pedestal values. For a laser beam reasonably well-centred on the sensor and perpendicular to the sensor plane, the strip signals follow a gaussian distribution. Full details on how the position measurements are made in the final system are given in Section 5.

As originally noted by Kroha [7], the resolution for measurement of the laser

⁵ Point Source 5 mm outer diameter stainless-steel jacket fibres.

beam position could be improved by correcting for variations in the thickness of the amorphous silicon layer and the glass substrate. Such variations may lead to interference patterns in the transmission and absorption of the laser light thus affecting the beam position measurement, see also Bauer et al [8]. Correction matrices with a $250\ \mu\text{m}$ grid were measured for all sensors. Using the correction matrices, the best resolution obtained in the test setup was less than $2\ \mu\text{m}$ – details are given in reference [2]. However, it was decided not to use the correction matrices in the routine analysis of the laser data as other systematic effects were much larger. These will be discussed in Section 5.

4 Readout and control

The photo-current signals from the sensor strips are carried from the MVD by the special cables described in Section 3.1 via the patch-boxes to the readout cards. For each of the eight z -locations along the MVD support tube all five TSD sensors are read out by a single card and all the cards are located in a VME crate at the MVD services area. There the signals are multiplexed, amplified by a current-voltage transformer, digitised and stored in memory on VMEbus boards. This memory is addressed using a complete rewrite of the VME driver to exploit Motorola's TUNDRA chipset [9,10]. The data are transferred via TCP/IP and made available to the ZEUS event building components.

The laser alignment slow control and data acquisition are fully integrated into the existing ZEUS MVD framework [4], which is based on VME board computers running Lynx OS and Intel PCs running SuSE GNU/Linux. This slow control incorporates an interface to the ZEUS safety control system prohibiting operation of the lasers when the beam lines are accessible to people.

The readout and slow control systems have been designed to allow two modes of operation [11]. For the first the laser system is fully integrated with the ZEUS run control system, data taken is stored on tape as part of the main ZEUS data store. It is then available for analysis along with the slow-control and general environmental records from normal data-taking. For the second mode the system can run in parallel with normal ZEUS data taking, but the laser data is now stored on disks on the Intel PC's via NFS. ASCII format copies of laser data from both data-taking modes are also stored on a local MVD computer disk.

5 Data analysis and first results

The raw data from a single laser run comprises two sets of ADC counts for both local x - and y -coordinate strips at each sensor plane along all five beam lines. The first set is taken with the laser shutters closed to establish the pedestal values, followed by the second set with shutters open. The raw signals are then given by subtracting the pedestal values from the ‘laser-on’ values. Early studies of the laser alignment data showed that typical values for the dark currents of the anode and cathode strips were around 0 and up to 50 ADC counts, respectively. A number of cuts and corrections were applied to strip signals, I_i , after pedestal subtraction and before applying the position algorithm:

- negative strip currents ($I_i < 0$) set to zero;
- isolated ‘hot strips’ with $I_i > 1000$ counts set to zero;
- strips with large ratios to both neighbours (I_i/I_{i+1} and $I_i/I_{i-1} > 10$) rejected;
- ‘empty’ sensor plane with $\sum_{i=1}^{16} I_i < 160$ counts rejected;
- to avoid edge effects the first two and last two strips are ignored.

5.1 Mean position

Two methods for determining the mean position, \bar{x} , and resolution, σ , of the signal in a sensor plane were considered. The simplest is to use a current weighted mean

$$\bar{x} = \sum_i x_i w_i \quad \text{with} \quad w_i = \frac{I_i}{\sum_i I_i} \quad \text{and} \quad \sigma = \frac{d}{\sqrt{12}} \sqrt{\sum_i w_i^2},$$

where $d \approx 300 \mu\text{m}$ is the strip width. The strip position, x_i , is taken to be at the centre of the strip and the error is assumed to be uniformly distributed over the strip width. This gives a conservative value of around $40 \mu\text{m}$ for the mean position resolution. A more sophisticated approach is to assume a gaussian profile for the strip-current distribution of a sensor plane. The parameters \bar{x} and σ are determined by fitting the profile to $N \exp[-(x - \bar{x})^2/(2\sigma^2)]$, with the error on an individual strip position taken to be $1/\sqrt{I_i}$. The fit is performed twice, with the second fit scaled to enforce $\chi^2/\text{ndf} = 1$. The typical resolution from the fit method is below $10 \mu\text{m}$. In more detail, an analysis of about 2580 position measurements showed that 95% of the errors were below $15 \mu\text{m}$, with a mean of $6.5 \mu\text{m}$, with the remaining 5% of errors extending up to $40 \mu\text{m}$. The gaussian fit method is the one used for all the results described below. Fig. 6 shows the beam-profile signals and gaussian fits along one beam line. The attenuation of the laser intensity and beam broadening are evident as the

number of sensors traversed increases. The attenuation is roughly consistent with the 80% transmission found in the test system.

The mean positions may be plotted in sensor local coordinates or in ZEUS coordinates. The geometrical relationship between them is shown Fig. 7 and the transformation from the local system, \mathbf{r}_{local} , to the common ZEUS system, \mathbf{r}_{ZEUS} may be written as

$$\mathbf{r}_{ZEUS} = \mathcal{R} \cdot \mathbf{r}_{local} + \mathcal{T}$$

where \mathcal{R} is a 2×2 rotation matrix and \mathcal{T} a 2-D translation. The transformations also take into account the standard or reversed orientation of the sensors.

During the period January to August 2004, laser data were collected regularly at the end of each HERA fill for normal e-p interactions, giving a total of 200 runs. The first attempt at analysis compared the mean sensor positions of a given laser beam relative to a reference run – usually the first run of the period under study. The reason for plotting positions relative to a reference run is to allow the data from different beams to be plotted using a common scale. An example of the data for the whole period is shown in Fig. 8.

The figure shows the relative mean position of the y , anode, signal along laser beam-3 in each of the sensor planes, with plane 0 (RCTD) at the top and plane 7 (FCTD) at the bottom. A number of points may be made:

- the size of deviations tends to increase with distance along the laser beam;
- there are some quite large deviations in planes 5, 6, 7, up to $100 \mu\text{m}$ or so;
- there are clear correlations between the larger deviations in different planes.

Although not shown, the local x -coordinate (cathode) signals shows similar features but with smaller fluctuations. The difficult question to answer from this type of plot is whether this is evidence for movement of the MVD support tube or simply instabilities of the lasers and noise in the sensors. The data shown in the figure were collected from laser runs separated by quite long time intervals – hours or even days between consecutive runs. In between laser runs, the lasers were switched off. The lasers were switched on for a short while before an alignment data run, but there was insufficient time to ensure that the system had stabilised because of the exigencies of physics data-taking.

For these reasons an alternative procedure was developed for the analysis of the laser beam position data. The idea, to define each beam line as an independent ‘straightness monitor’, is shown schematically in Fig. 9. For a given laser beam and local coordinate the mean positions in sensor planes 0 and 7, attached to the CTD, are used to define the reference straight line. The expected position of the beam at a sensor plane, i , within the MVD, is then

given in local sensor coordinates by:

$$x_i = x_0 \frac{z_i - z_7}{z_0 - z_7} + x_7 \frac{z_0 - z_i}{z_0 - z_7}, \quad y_i = y_0 \frac{z_i - z_7}{z_0 - z_7} + y_7 \frac{z_0 - z_i}{z_0 - z_7}.$$

The *residuals* in the two coordinate directions are calculated as the differences between the expected positions and the corresponding measured mean positions, $(x_i - \bar{x}_i^{meas.})$, $(y_i - \bar{y}_i^{meas.})$. Fig. 10 shows the same data as displayed in Fig. 8, but now the residuals are plotted relative to the line defined by planes 0 and 7 (hence the absence of deviations at these positions). The residuals are plotted relative to those from a reference run, which is chosen to be the same as that used for these data before. Comparing Figs 10 and 8, one sees that the fluctuations are smaller, particularly in the planes furthest from the optical fibre laser heads. There is evidence for movement or for further instabilities of the lasers. More information is clearly needed.

There is quite a variation in the ‘noise’ level of individual laser beams, fluctuations are caused by pointing instability of the source and beam deflections from thermal gradients. Beam-3 shown in Figures 8 and 10 is relatively quiet. Allowing for this variation, similar features as described above are seen for the other beams in the system. Although there may be evidence for some movement, there is no evidence for any permanent ‘step changes’ in the position of the MVD support tube over the nearly nine months of data considered in this section. If the residuals for a given beam and sensor are plotted for the whole period, the resulting distributions are reasonably gaussian with values of σ around 10 – 20 μm for a ‘quiet’ laser beam and around 40 – 50 μm for a ‘noisy’ beam.

6 Correlation studies

As discussed in the preceding section, to establish whether the variations in mean position (residual) of a sensor are caused by motion, more information is needed. The first attempts to provide precision alignment constants for the MVD tracking sensors used events with through-going cosmic ray tracks only. There were two sources for the data sets: the first from dedicated cosmic-ray runs with a special trigger taken when the HERA collider was not operational and the second from cosmic-ray events selected from the normal e-p interaction data stream with HERA operational. It was expected that the two types of data would give the same results (provided that the data were collected during roughly the same period of time and that no changes were made to the detector configuration). They did not and no ‘trivial’ explanations could be found for the differences in alignment constants which were of magnitude

50 – 100 μm . It was eventually realised⁶ that there was a difference in the environmental conditions: whether the HERA collider magnets were powered on or not. As described in Section 2, the final focusing GG magnet in the HERA-II configuration reaches well within the detector and quite close to the central tracking system. In addition, the MVD readout and services cables are tightly wrapped around it. The way the magnet is supported within the detector is by a strap from above and this would allow some movement, indeed position sensors attached to the magnet showed that it does move slightly.

Two further steps were required before this idea could be tested quantitatively: the first was to change the mode of operation of the laser system and the second was to get access to the temporal records of the GG magnet current. To reduce laser instabilities from switching the lasers on and off, it was decided to leave the lasers on permanently (while the detector was closed for data taking) and control laser runs by the mechanical shutter. With this change laser runs could be taken at much shorter intervals. To study possible external effects, the laser data were collected every 4 minutes for periods of hours, up to a maximum of nine days. These data sets gave ample opportunity for study of the effects of both regular and irregular operation of the ZEUS detector. The circulation of bunches in HERA provides a very accurate clock signal that is used for synchronisation both within the ZEUS experiment and between the experiment and HERA, so it was relatively straightforward to relate the state of the GG magnet current to the timing of laser runs.

Other sources of environmental change were also considered, such as the temperature of the MVD, the temperature of the beam pipe and the temperature of the CTD. The last two were quickly ruled out, but it was found that the temperature within the MVD could change by almost 10°C depending on whether the onboard electronics were powered or not.

Fig. 11 shows an example of the results from the correlation studies. It shows the local- x (cathode) coordinate residuals for laser beam-2 at the five planes within the MVD (upper five plots) together with the GG magnet current and the MVD temperature in the lowest two plots. All are plotted against the common elapsed time synchronised by the HERA clock. Note that the residuals are the actual values, relative to the beam-2 laser line, at each measuring plane and not relative to a reference run. The temperature in the MVD is measured at a position near wheel-3. Fig. 12 shows a similar plot from the same runs for the local- y (anode) coordinate residuals.

Considering the magnet current first, Fig. 11 (local- x) shows that between times of 0 and 45000 s there is a correlation in time between the mean residual values themselves and with the magnet current being zero or non-zero. There

⁶ We thank Drs R. Carlin and U. Koetz for making this suggestion.

is also a tendency for the size of the movement to increase with increasing plane index. Fig. 12 (local- y) shows a similar, but more pronounced correlated movement. This pattern of movement is also seen in the data from other laser beams and is consistent with the MVD support tube being tilted about a fulcrum near the rear CTD attachment. The assumption is that the MVD support tube moves when the GG magnet moves, via the MVD cables.

Regarding correlated movement with temperature, the evidence is very clearly seen in the local- y plots (Fig. 12) for times between 50000 and 65000s. The changes in temperature occurs when the MVD electronics are switched on or off. The pattern of movement is different in detail to that related to the GG magnet motion, the biggest effects are now seen in the three sensor planes nearest to the on-detector electronics, at planes 2, 3 and 5 (MVD barrel flanges and wheel-3). Fig. 11 – local- x coordinate for beam-2 – shows a much less clear correlation. The concentration of movement at these three sensor planes is also seen in other beam line data.

Figs 13 and 14 show the same beam-2 data but now the residuals have been transformed to the global ZEUS x - and y -coordinates, respectively. At this beam position the GG magnet associated movement is mainly along the ZEUS y -axis, whereas the MVD temperature movement is seen in both global x and y directions. Originally it was thought that one might be able to deduce the nature of the movement of the support tube by fitting the pattern of local movements to changes expected from a set of ‘standard motions’ – for example twists and sags. This might well have been unrealistic even with the full production system as designed, but it is impossible with reduced number of beam lines and reliable sensors. However the system is able to give some quantitative information on the magnitude of local movements and to track such changes.

The residual plots indicate that the position of a sensor is stable while the external conditions are stable and that the positions of stability are themselves stable and reproducible. This has been investigated in more detail by averaging the residuals for periods of stability during long laser runs. The periods are defined by external changes, but regions of rapid change are excluded. Results from a typical long period of runs are shown in Fig.15. Two long periods, corresponding to e-p data-taking when both the MVD and GG magnet are on can be seen. In between is a period of beam injection and acceleration when the MVD is off throughout and the GG magnet current is varying, but has two short periods when it is also off. This pattern is typical and shows that ‘off’ periods are shorter than those when everything is on.

The detailed results depend on the noise quality of lasers and the sensors. For beams 2, 3 and 4 most residual means have RMS values better than $10\ \mu\text{m}$, beam 1 is noisier and the local- x residuals at plane-6 appear to be unstable.

The positions for normal running with both the MVD and GG magnet powered and those with both MVD and GG magnets off are of particular interest. The results for local coordinates and beam 2 are shown in Fig. 16. Each point shows the mean and standard deviation (shown as a vertical error bar, often smaller than the symbol size) for a data set corresponding to a single period of stability. The means for the MVD and GG magnet both on are shown as triangles and when both are off as circles. The data show clearly that the structure is moving between two well-defined positions ‘ON’ and ‘OFF’. The movement is mainly in the local- y coordinate and can be as much as $120\ \mu\text{m}$.

Fig. 17 shows the same results but now plotted for x - and y -residuals in the ZEUS coordinate frame. At this beam position, the size of the shift between ON and OFF positions is largest in the y direction but there is also a smaller but non-zero shift along the x direction. Two other positions are shown as single points on these plots: the 8th point, shown as a square, is for the MVD on and GG magnet off and the last point of all (inverted triangle) is for the MVD off and GG magnet on.

To give a more quantitative estimate of the movements, the beam-2 means from Figs 16 and 17 have been averaged over the 16 ON periods and the 14 OFF periods shown. The difference in the mean values for a given beam and sensor position shows the size of the movement and the standard deviations give a good idea of how precisely the MVD support frame is able to return to a particular position. These results are collected in Table 3. Movements of over $100\ \mu\text{m}$ in the local frame are seen, with the largest standard deviations on the difference in position around $10\ \mu\text{m}$. A similar analysis has been performed for beam-4 residuals and the results are shown in Table 4. The movements seen at the position of beam-4 are smaller than those at beam-2, but there is clear evidence for two stable positions with standard deviations on the differences of position again at most $10\ \mu\text{m}$.

7 Summary

This paper has described the laser alignment system for the ZEUS microvertex detector and given a summary of its performance. The infra-red lasers and semi-transparent sensors provide five ‘straightness monitors’ that can detect movement of the MVD support structure at the level of $100\ \mu\text{m}$ or better. The system has been working reliably since it was installed and commissioned in 2001. The one less than satisfactory feature is the way that the optical fibre heads are mounted on the central tracking detector. Due to constraints of time, space and money, a rather crude system had to be employed which made it difficult to adjust the pointing of the laser beams, even at the time of installation, and impossible thereafter.

Time-series analysis of the residuals of the laser beam position with respect to the straight lines derived from the positions of a beam at the sensors mounted on the front and rear of the central tracking chamber is how the laser alignment information is used.

From the studies reported in this paper, the following conclusions may be drawn:

- The MVD support structure is very stable and there is no indication of any large long-term movement or step change (over the period 2003 to 2007);
- When external conditions vary, particularly the GG magnet on or off and the MVD on-detector electronics being powered or not, the MVD support structure shows movements locally as large as $100\ \mu\text{m}$;
- Once the conditions return to the previous state the MVD support tube returns to its previous configuration, to within $10\ \mu\text{m}$.

Finally, it is clear that track data for precision alignment should be collected under the operational conditions of regular e-p interaction data taking.

Acknowledgements

We thank H. Kroha and the Munich group for help and advice during the early stages of this project. We thank T. Handford for his invaluable help throughout. We thank J. Hill for outstanding effort during the design, construction and installation of the laser system. We thank C. Band, D. Smith and the Oxford Photo-Fabrication Unit for their help with the design and manufacture of the flat readout cables. We thank S. Boogert, and M. Rigby for their work on the prototype system and L. Hung for her help in analysing early production data. Finally we thank C. Youngman for help and advice on how to access HERA and ZEUS slow-control data.

References

- [1] The ZEUS collaboration, DESY-PRC 97/01, (1997).
- [2] T. Matsushita *et. al.*, *Nucl. Instrum. Methods A* **466**, (2001) 383.
- [3] E. N. Koffeman, *Nucl. Instrum. Methods A* **453**, (2000) 89.
- [4] ZEUS MVD Group, *The design and performance of the ZEUS MVD*, to be submitted to *NIM A*.
- [5] W. Blum, H. Kroha and P. Widmann, *Nucl. Instrum. Methods A* **367**, (1995) 413.

- [6] <http://www.point-source.com/>
- [7] H. Kroha, *Nucl. Phys. B* **54**, (1997) 80.
- [8] F. Bauer *et. al.*, *IEEE Trans. Nucl. Sci.* **48**, (2001) 262.
- [9] A. Polini, *UVMElib*, ZEUS Note 99-071 (1999), unpublished.
- [10] “The Architecture of the ZEUS Microvertex Detector DAQ and Second Level Global Track Trigger.”, A. Polini, talk given at 2003 Conference for Computing in High-Energy and Nuclear Physics (CHEP 03), published in eConf C0303241:MOGT005,2003 e-Print Archive: physics/0307006
- [11] J. Ferrando & C. Youngman, *The MVD laser alignment System Guide*, ZEUS Note 05-013 (2005), unpublished.

List of Figures

- 1 Layout of the ZEUS MVD along beam axis. The barrel part covers the interaction region. Four wheels cover the forward direction of the proton beam. 17
- 2 Cross sections of the MVD. Left and right are barrel and wheel, respectively. The coordinate system is that of the ZEUS experiment, with the z -axis along the proton beam direction, the x -axis pointing towards the centre of the HERA ring and the y -axis vertical. 18
- 3 Schematic diagram of one laser alignment beam and sensors. Forward and Rear refer to the orientation of the tracking detectors, with forward in the direction of the HERA proton beam. The sensor numbering is also shown. 19
- 4 Top figures: the standard and reversed sensor orientations. Bottom: photo of a standard sensor showing the bonding of the flat readout cables. 20
- 5 The positions and numbering of the five laser beams around the circumference of the MVD support tube. View is from the forward end of the CTD in the ZEUS coordinate system. 21
- 6 Examples of the beam-profile signals from the sensors along one beam line, together with the gaussian fits. The strip currents are in units of ADC counts and are plotted as functions of strip number. RCTD corresponds to sensor plane 0 and FCTD to sensor plane 7 – see Table 1 for details. 22
- 7 The orientation of sensor local coordinates with respect to the ZEUS coordinate system, viewed from the rear CTD end. The labels S and R refer to standard and reversed sensors, respectively. 23
- 8 Relative positions of laser beam-3, in local coordinates, at the seven planes starting with plane-0 at the top. The y (anode) signals are shown as functions of the run number. At the time of these measurements the laser at beam-3 was that with the highest power. 24

9	The procedure used to define the reference line for a given laser beam using the CTD planes 0 and 7 and residual (offset) between the expected position and measured mean position in an interior MVD sensor plane.	25
10	Residuals of laser beam-3, in local coordinates, with respect to the straightness monitor defined by the laser-beam positions in planes 0 and 7 (R and FCTD). Other details the same as in Fig. 8.	26
11	Local- x (cathode) residuals for beam-2, planes 1, 2, 3, 5 & 6 with the GG magnet current and the MVD temperature in the bottom two plots, all as a function of elapsed time.	27
12	Local- y (anode) residuals for beam-2, planes 1, 2, 3, 5 & 6 with the GG magnet current and the MVD temperature in the bottom two plots, all as a function of elapsed time.	28
13	ZEUS frame x -residuals for beam-2, planes 1, 2, 3, 5 & 6 with the GG magnet current and the MVD temperature in the bottom two plots, all as a function of elapsed time.	29
14	ZEUS frame y -residuals for beam-2, planes 1, 2, 3, 5 & 6 with the GG magnet current and the MVD temperature in the bottom two plots, all as a function of elapsed time.	30
15	Residuals for local- y (dark grey left-hand scales) and local- x (light grey right-hand scales) are shown for two periods of e-p data-taking with MVD and GG magnet both on and a period in between when the MVD was off with the GG current being varied with two short sub-periods when it was also off.	31
16	Mean values of residuals for local- y (left-hand plots) and local- x (right-hand plots) for beam-2 during periods of stability. The symbols indicate different conditions: triangle MVD and GG magnet both on; circle MVD and GG both off; square MVD on, GG off (8 th data set only); inverted triangle MVD off, GG on (last data set in the sequence). The size of the standard deviation is shown by the vertical error bar.	32
17	Mean values of ZEUS global- y (left-hand plots) and global- x (right-hand plots) residuals for beam-2 during periods of stability. The symbols have the same meaning as for Fig. 16.	33

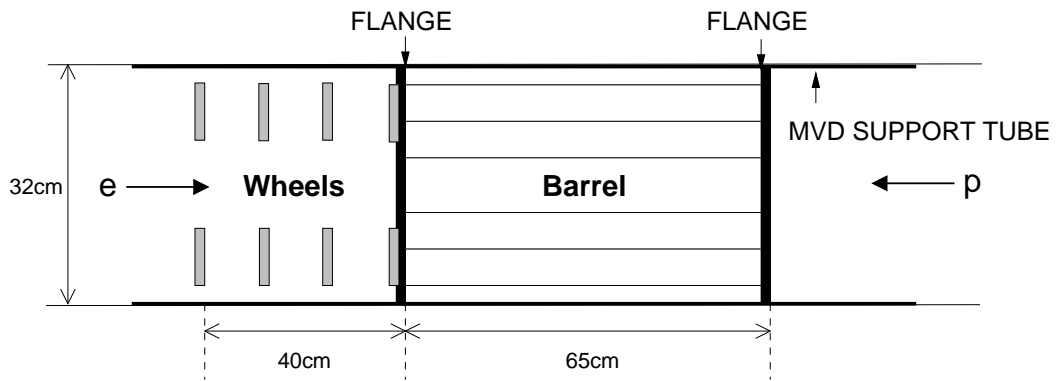


Fig. 1. Layout of the ZEUS MVD along beam axis. The barrel part covers the interaction region. Four wheels cover the forward direction of the proton beam.

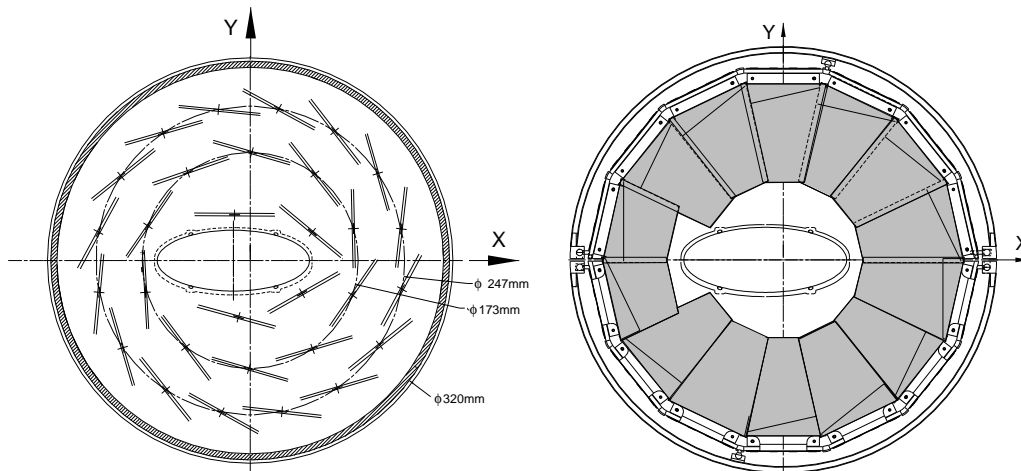


Fig. 2. Cross sections of the MVD. Left and right are barrel and wheel, respectively. The coordinate system is that of the ZEUS experiment, with the z -axis along the proton beam direction, the x -axis pointing towards the centre of the HERA ring and the y -axis vertical.

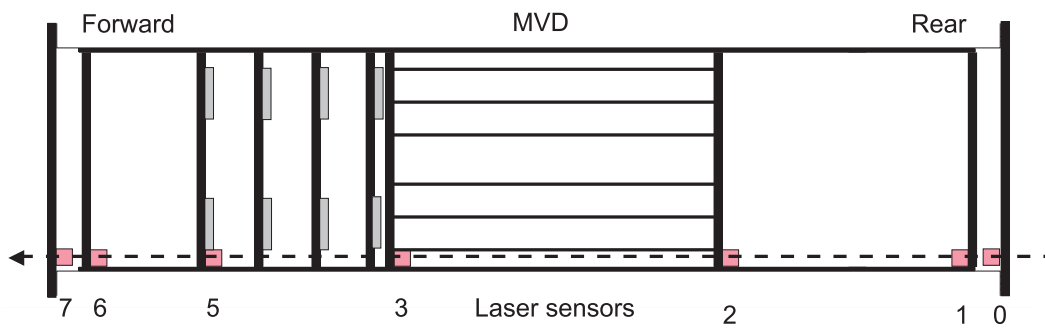


Fig. 3. Schematic diagram of one laser alignment beam and sensors. Forward and Rear refer to the orientation of the tracking detectors, with forward in the direction of the HERA proton beam. The sensor numbering is also shown.

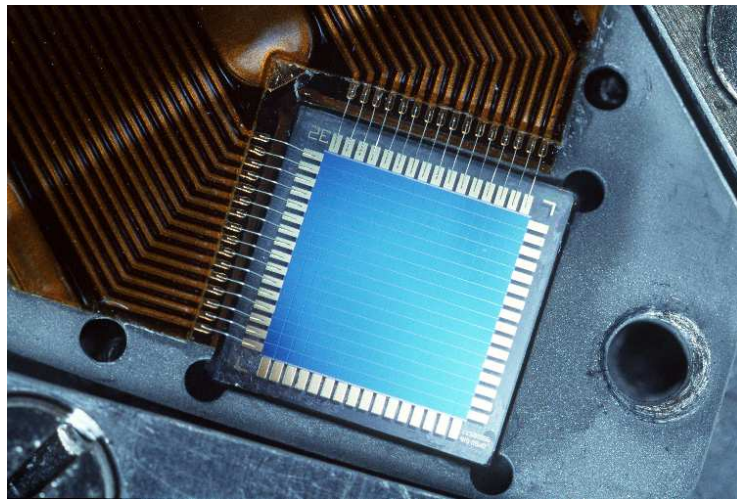
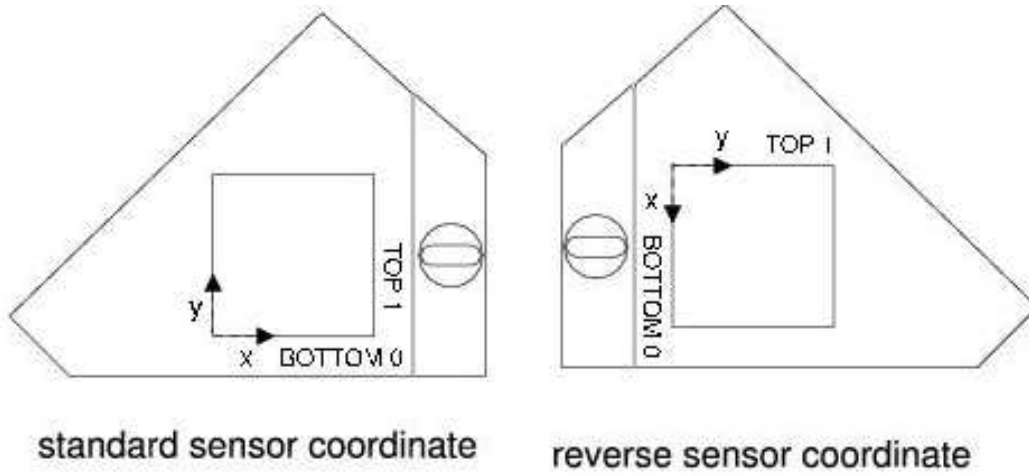


Fig. 4. Top figures: the standard and reversed sensor orientations. Bottom: photo of a standard sensor showing the bonding of the flat readout cables.

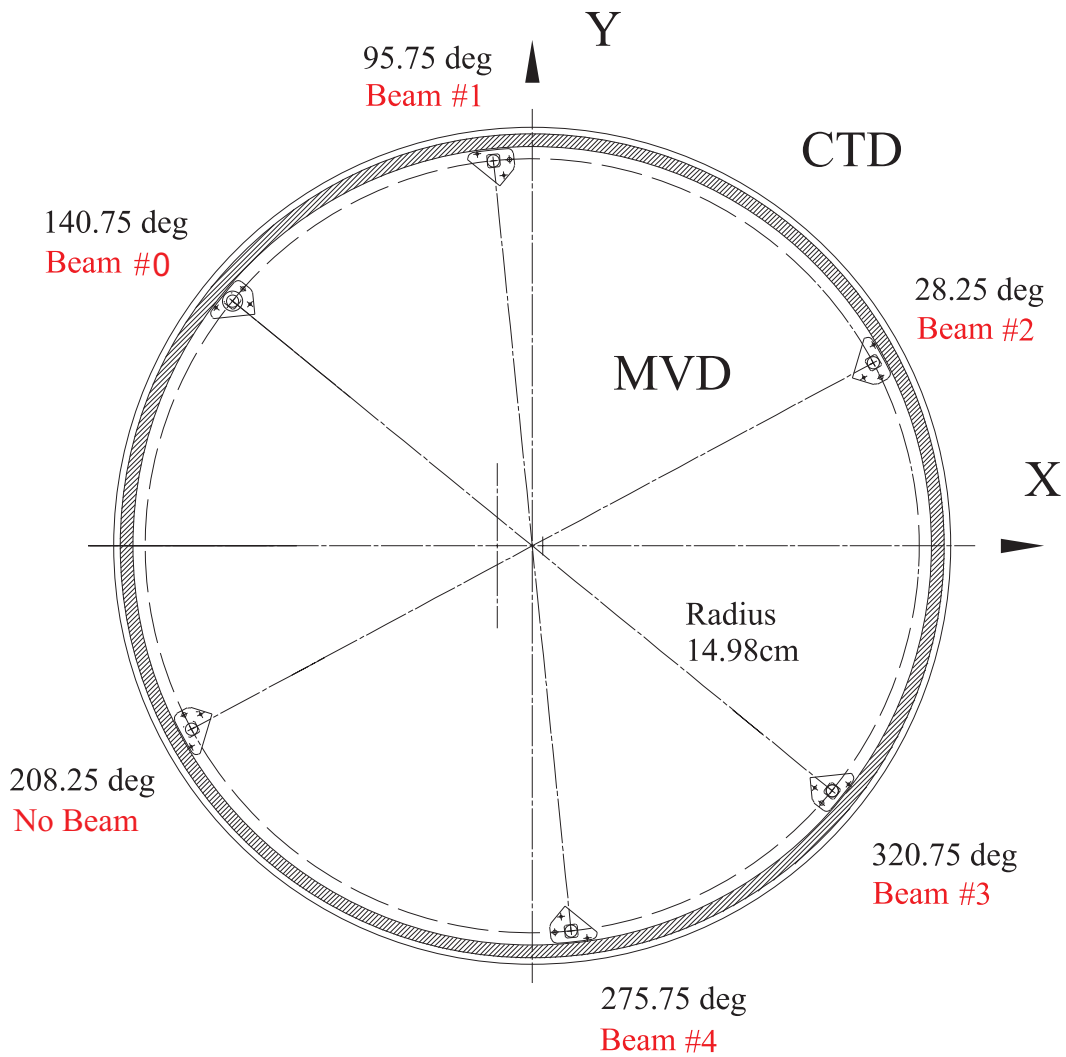


Fig. 5. The positions and numbering of the five laser beams around the circumference of the MVD support tube. View is from the forward end of the CTD in the ZEUS coordinate system.

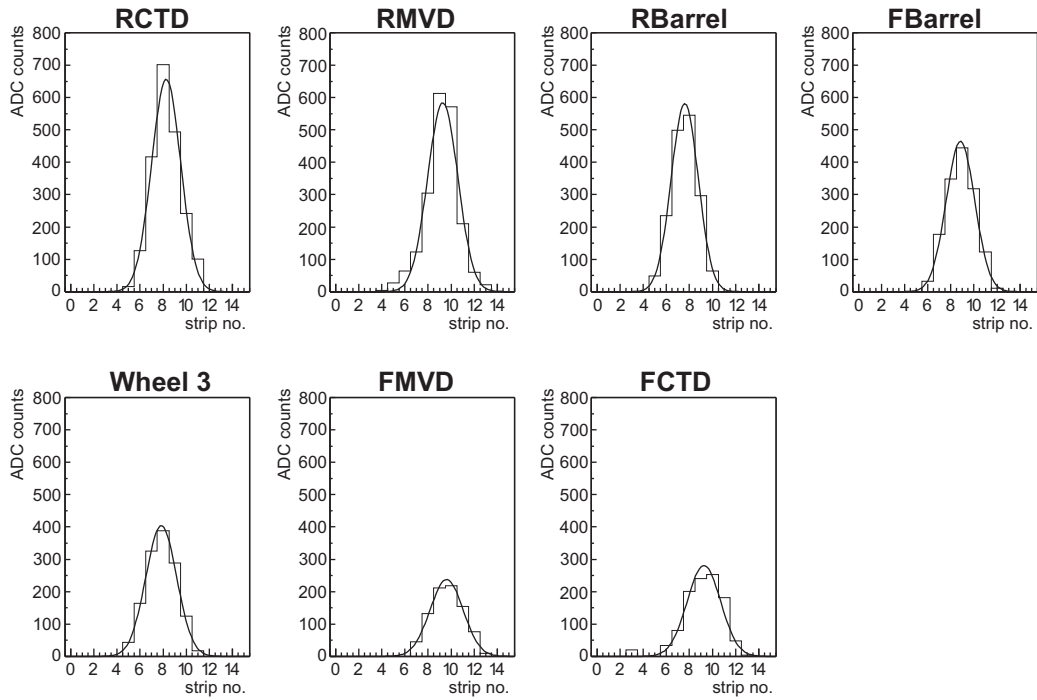


Fig. 6. Examples of the beam-profile signals from the sensors along one beam line, together with the gaussian fits. The strip currents are in units of ADC counts and are plotted as functions of strip number. RCTD corresponds to sensor plane 0 and FCTD to sensor plane 7 – see Table 1 for details.

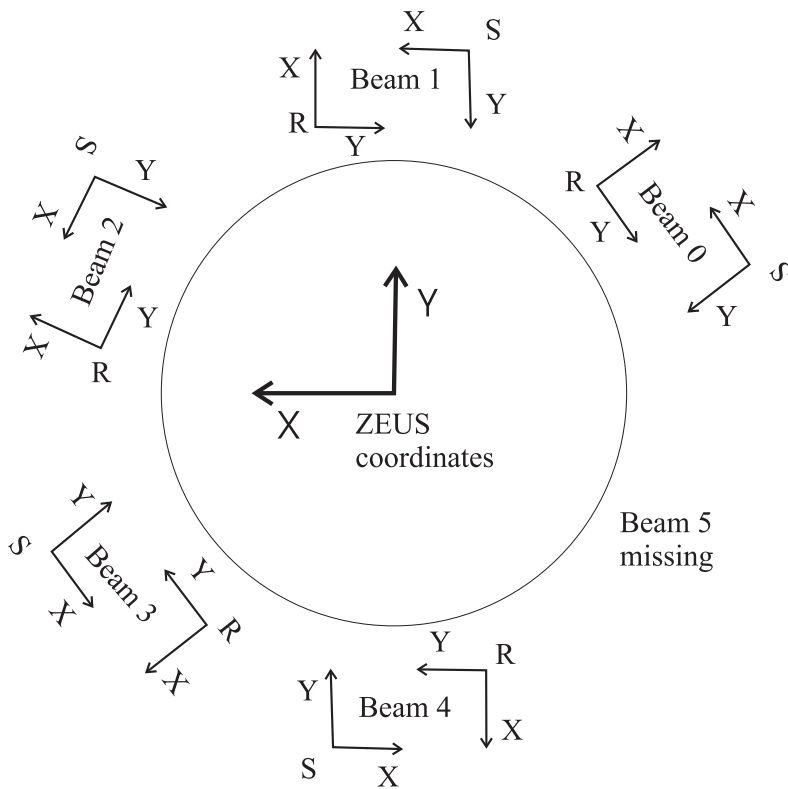


Fig. 7. The orientation of sensor local coordinates with respect to the ZEUS coordinate system, viewed from the rear CTD end. The labels S and R refer to standard and reversed sensors, respectively.

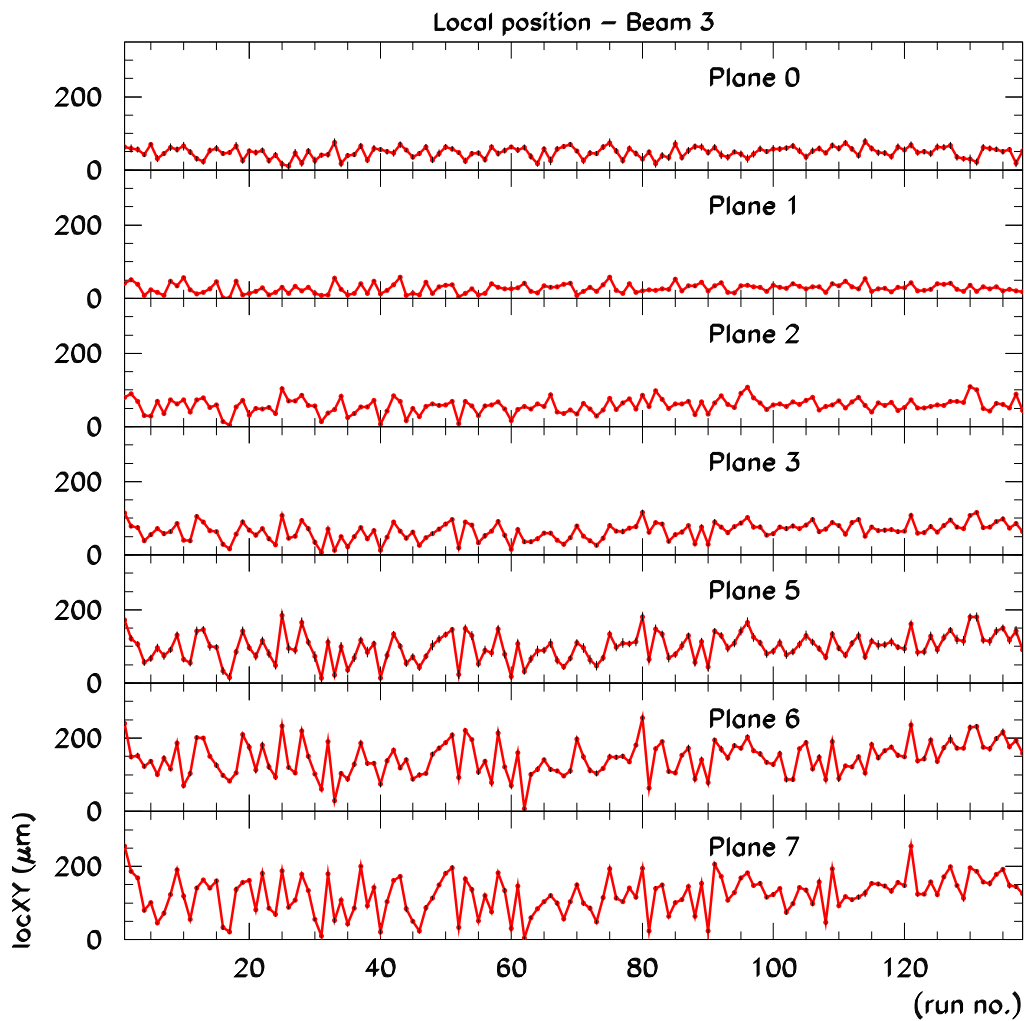


Fig. 8. Relative positions of laser beam-3, in local coordinates, at the seven planes starting with plane-0 at the top. The y (anode) signals are shown as functions of the run number. At the time of these measurements the laser at beam-3 was that with the highest power.

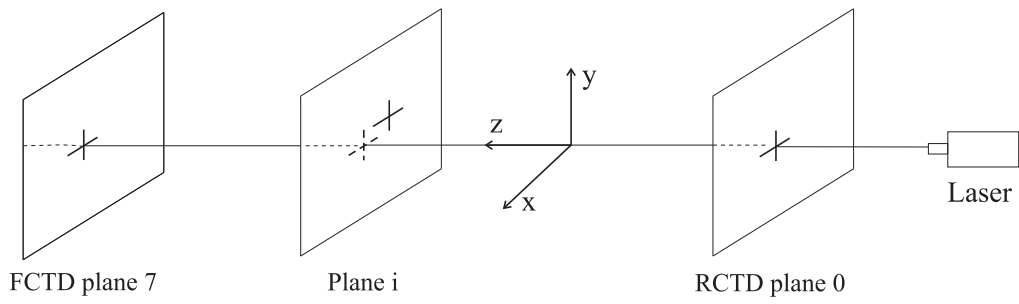


Fig. 9. The procedure used to define the reference line for a given laser beam using the CTD planes 0 and 7 and residual (offset) between the expected position and measured mean position in an interior MVD sensor plane.

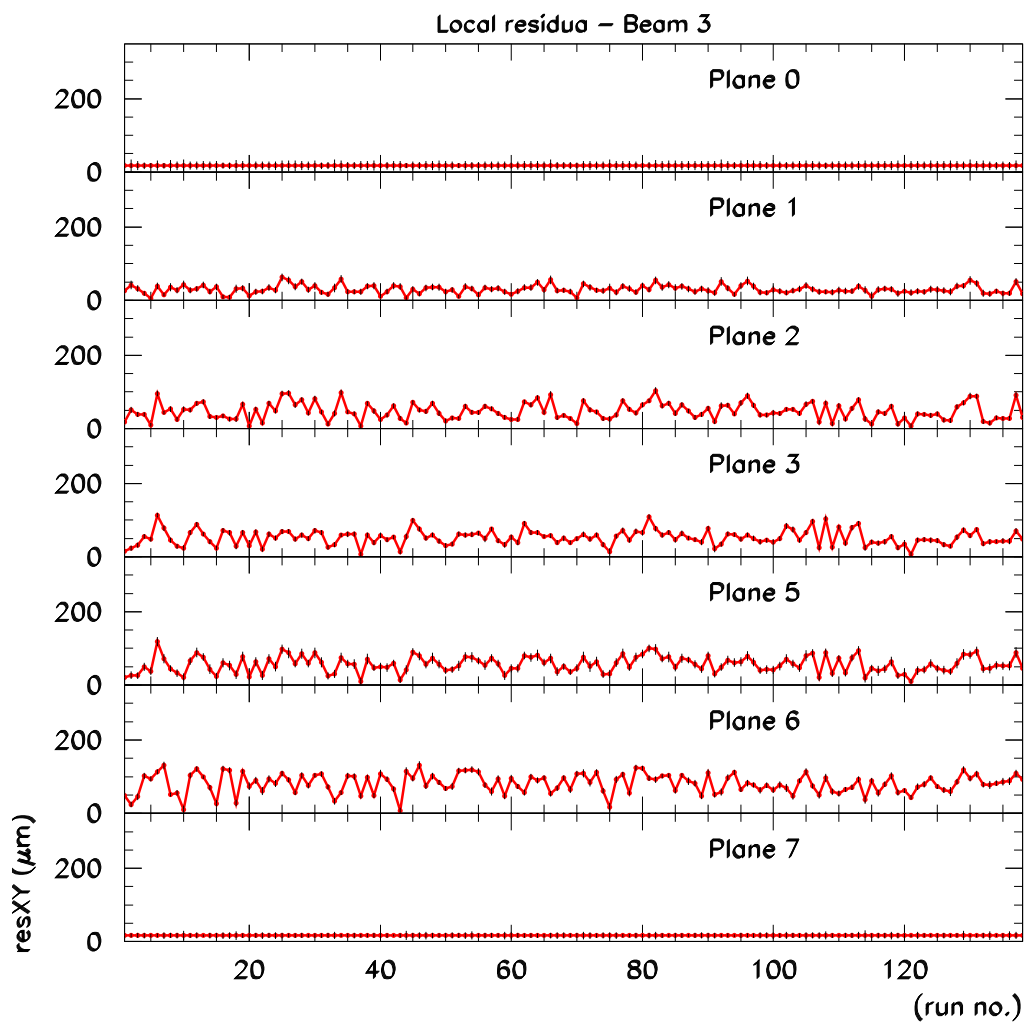


Fig. 10. Residuals of laser beam-3, in local coordinates, with respect to the straightness monitor defined by the laser-beam positions in planes 0 and 7 (R and FCTD). Other details the same as in Fig. 8.

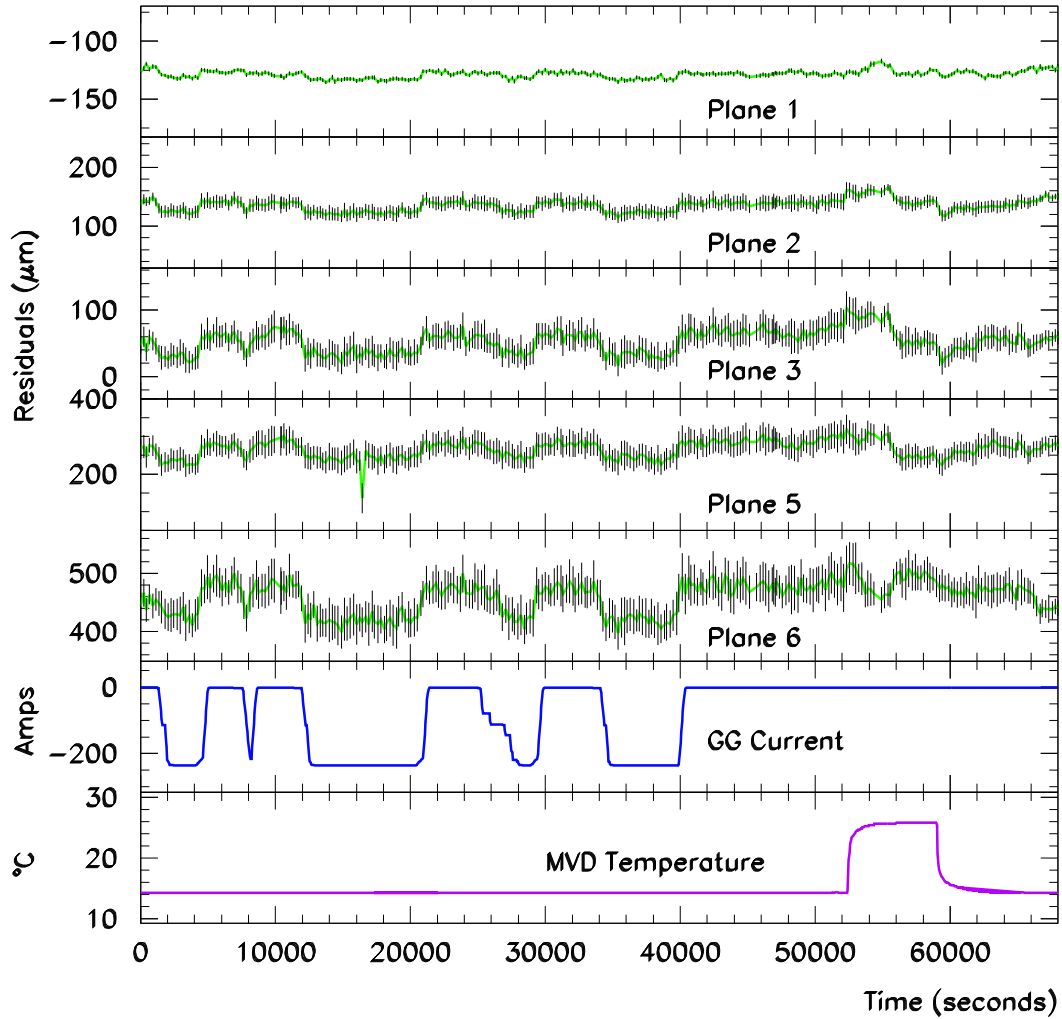


Fig. 11. Local- x (cathode) residuals for beam-2, planes 1, 2, 3, 5 & 6 with the GG magnet current and the MVD temperature in the bottom two plots, all as a function of elapsed time.

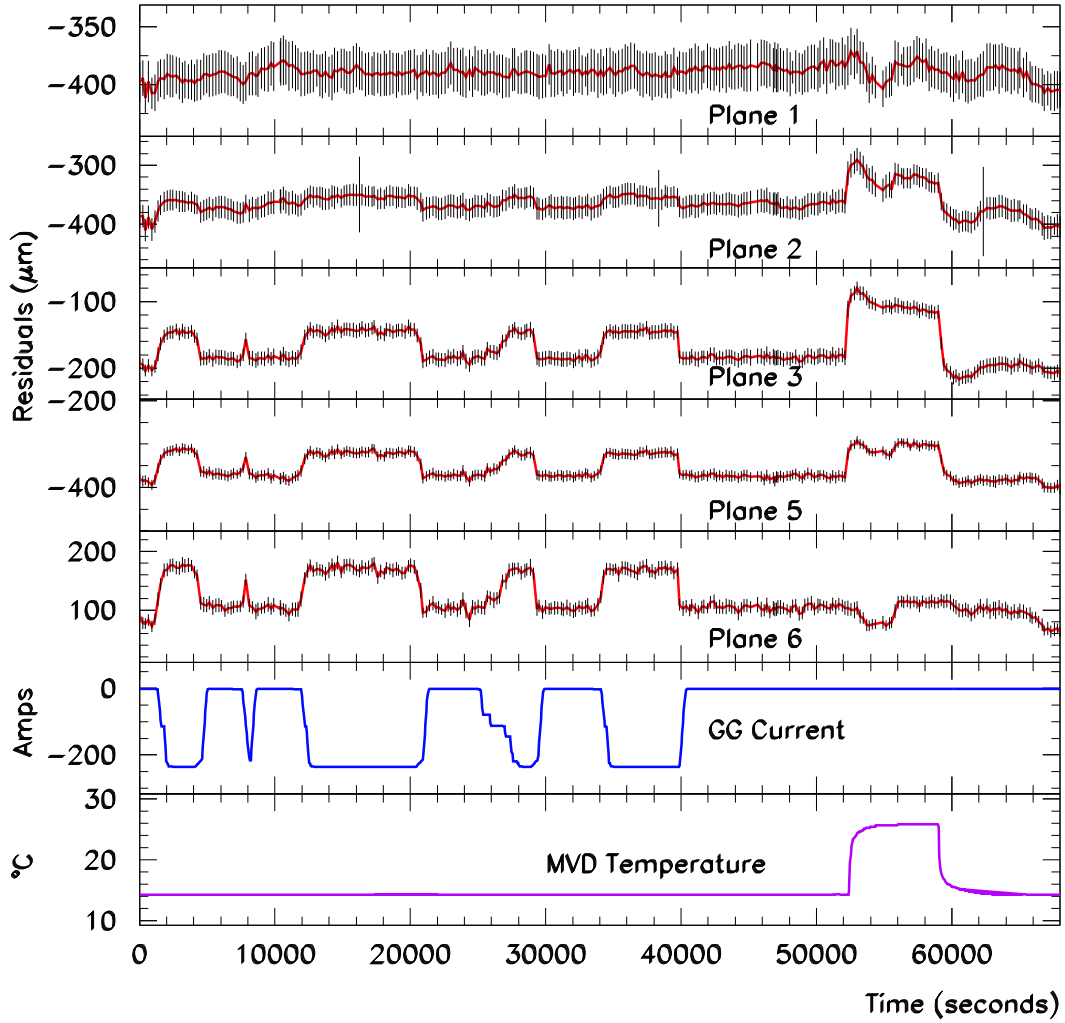


Fig. 12. Local- y (anode) residuals for beam-2, planes 1, 2, 3, 5 & 6 with the GG magnet current and the MVD temperature in the bottom two plots, all as a function of elapsed time.

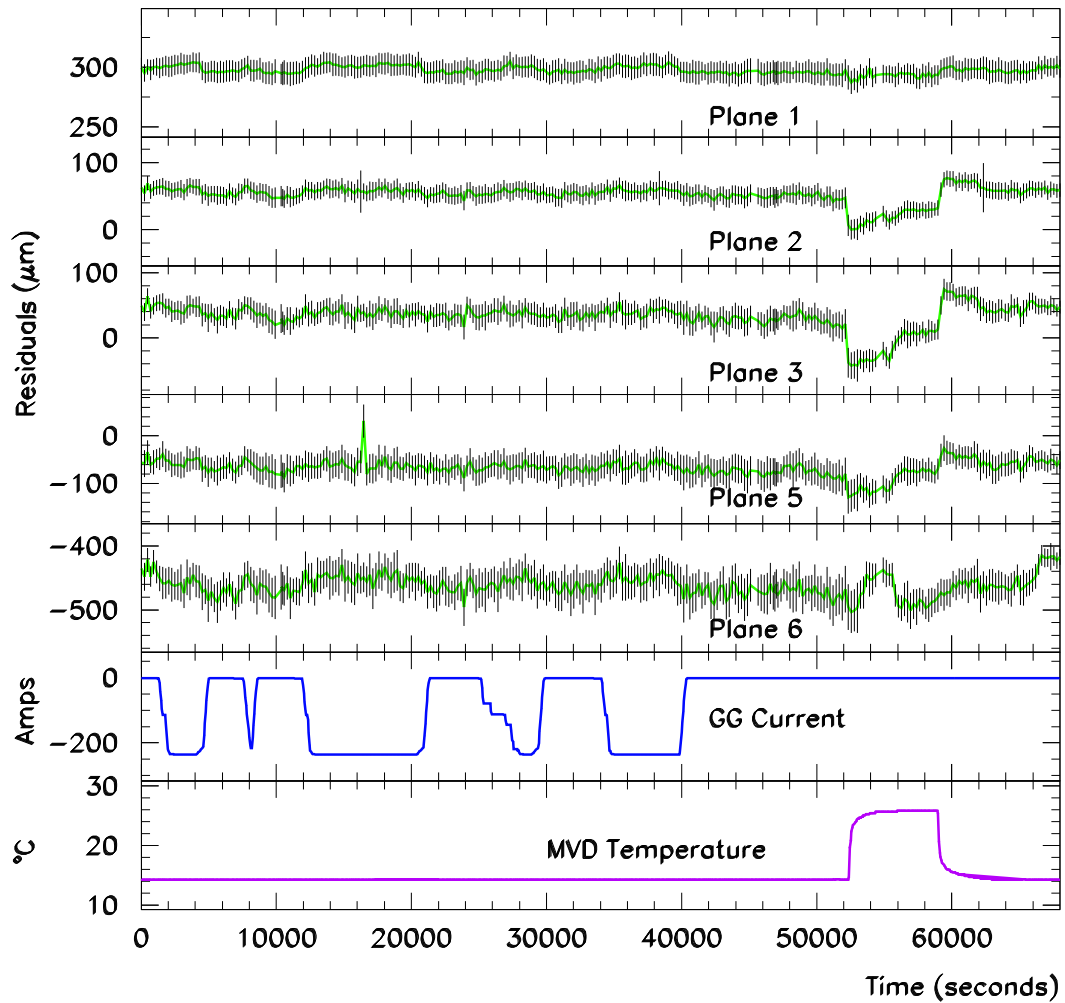


Fig. 13. ZEUS frame x -residuals for beam-2, planes 1, 2, 3, 5 & 6 with the GG magnet current and the MVD temperature in the bottom two plots, all as a function of elapsed time.

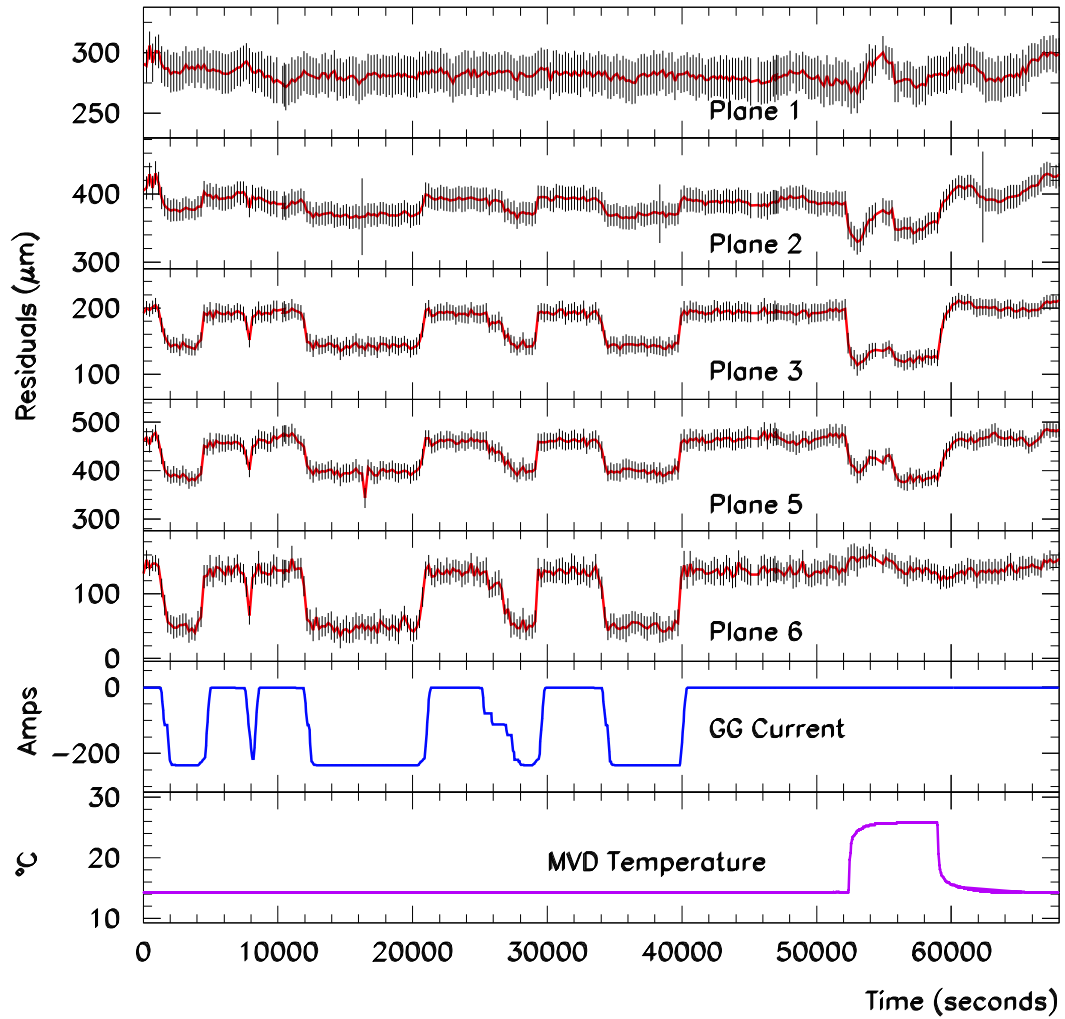


Fig. 14. ZEUS frame y -residuals for beam-2, planes 1, 2, 3, 5 & 6 with the GG magnet current and the MVD temperature in the bottom two plots, all as a function of elapsed time.

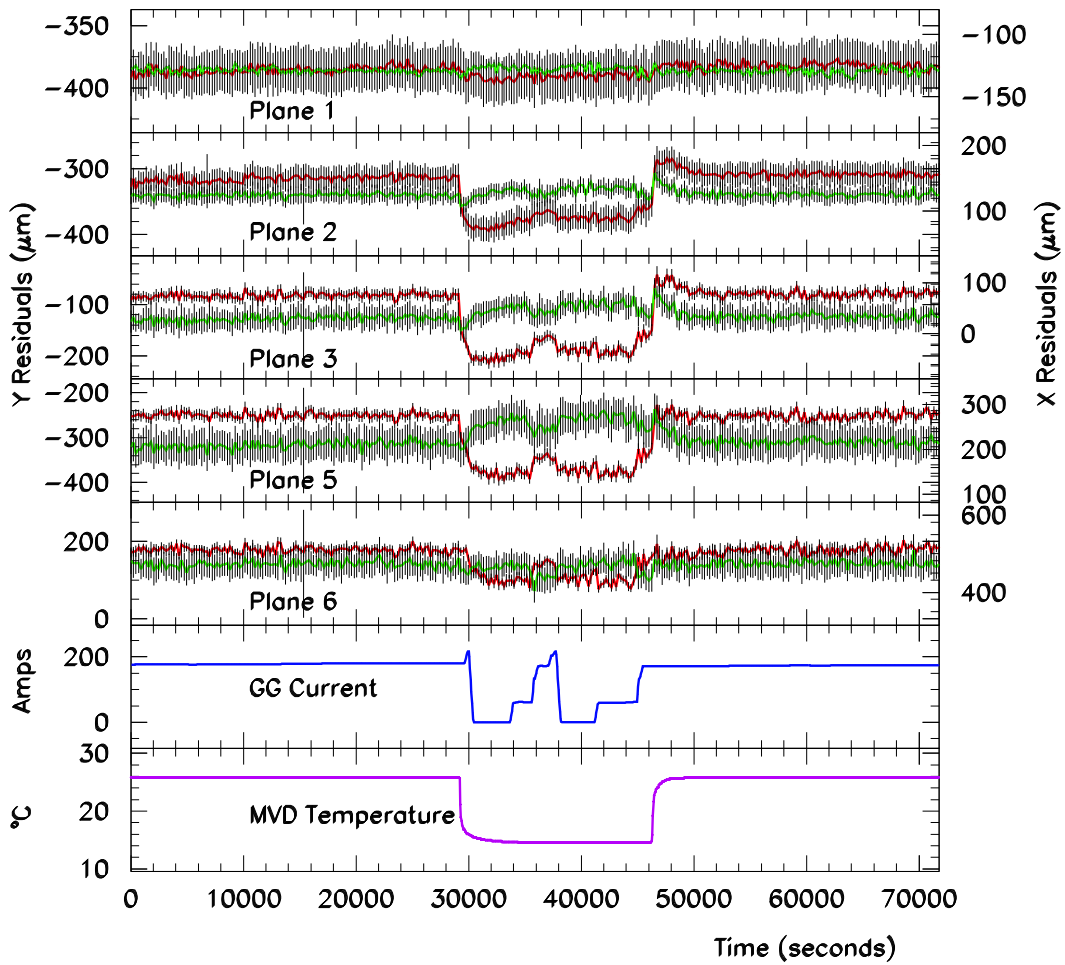


Fig. 15. Residuals for local- y (dark grey left-hand scales) and local- x (light grey right-hand scales) are shown for two periods of e-p data-taking with MVD and GG magnet both on and a period in between when the MVD was off with the GG current being varied with two short sub-periods when it was also off.

Beam 2

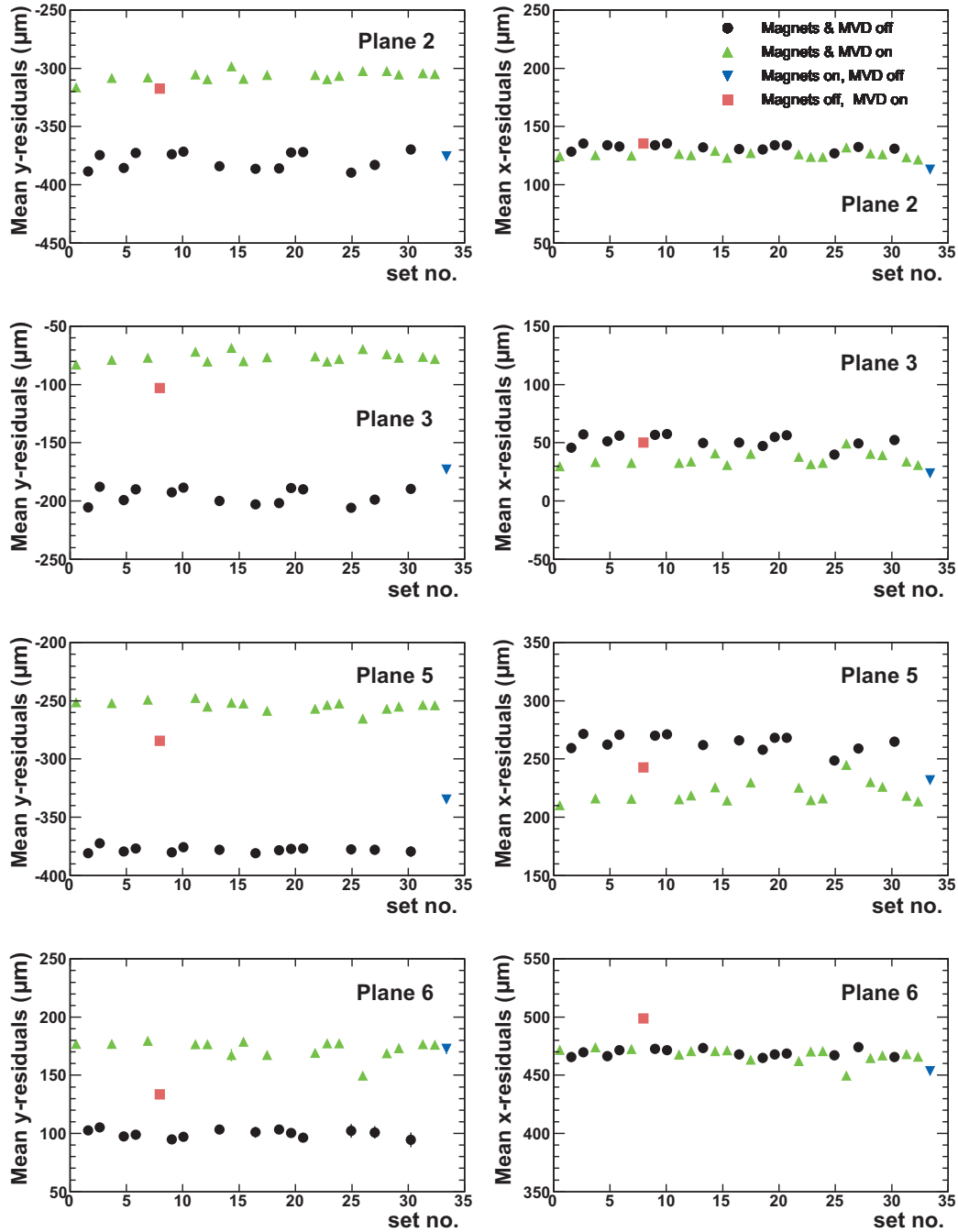


Fig. 16. Mean values of residuals for local- y (left-hand plots) and local- x (right-hand plots) for beam-2 during periods of stability. The symbols indicate different conditions: triangle MVD and GG magnet both on; circle MVD and GG both off; square MVD on, GG off (8th data set only); inverted triangle MVD off, GG on (last data set in the sequence). The size of the standard deviation is shown by the vertical error bar.

Beam 2

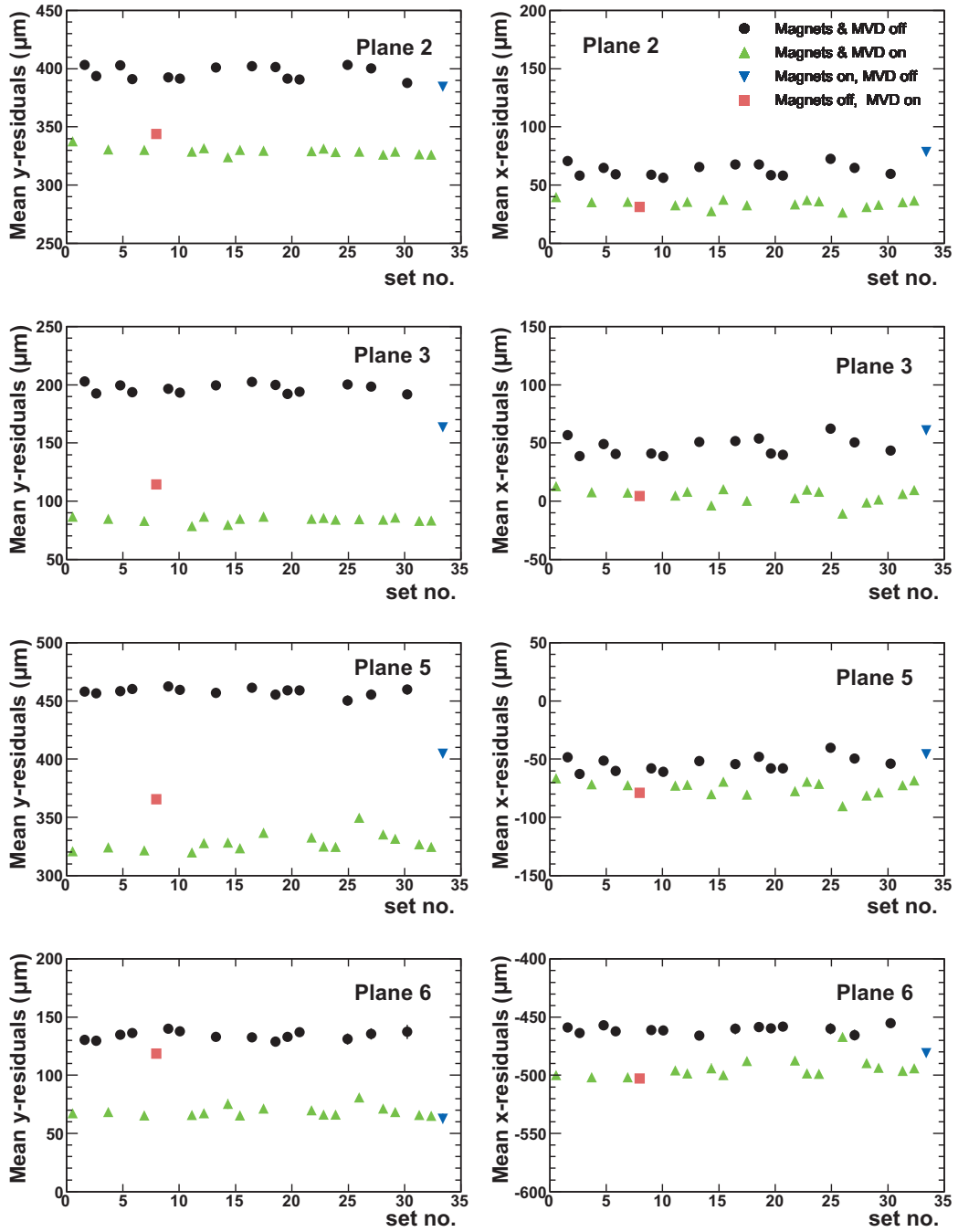


Fig. 17. Mean values of ZEUS global- y (left-hand plots) and global- x (right-hand plots) residuals for beam-2 during periods of stability. The symbols have the same meaning as for Fig. 16.

List of Tables

- 1 The positions of the sensor planes along the z -coordinate axis (parallel to the beam line) in the ZEUS reference frame with the origin at the nominal electron–proton interaction point. The plane positions are also shown in Fig. 3. 35
- 2 Laser beam positions, numbering and power. The details are from measurements made in April 2006. At this time some lasers were moved between beam lines, to get the best match between lasers and working sensors. 36
- 3 Mean and standard deviation, in microns, for the average of ON and OFF residuals for beam-2 at planes 2, 3, 5 and 6 and their differences in the local and global coordinate systems. 37
- 4 Mean and standard deviation, in microns, for the average of ON and OFF residuals for beam-4 at planes 2, 3, 5 and 6 and their differences in the local and global coordinate systems. 38

Table 1

The positions of the sensor planes along the z -coordinate axis (parallel to the beam line) in the ZEUS reference frame with the origin at the nominal electron–proton interaction point. The plane positions are also shown in Fig. 3.

Index	Plane		z (mm)	Comment
0	RCTD	Rear CTD end plate	−1078.1	reversed
1	RMVD	Rear MVD end flange	−1007.6	reversed
2	RBarrel	Rear MVD barrel flange	−360.4	standard
3	FBarrel	Forward MVD barrel flange	302.6	standard
4	Wheel-1		437.1	missing
5	Wheel-3	MVD wheel-3	717.1	standard
6	FMVD	Forward MVD end flange	1104.6	standard
7	FCTD	Forward CTD end plate	1179.1	standard

Table 2

Laser beam positions, numbering and power. The details are from measurements made in April 2006. At this time some lasers were moved between beam lines, to get the best match between lasers and working sensors.

Beam	Position	Power (mW)	Comment
0	140.75°	2.9	lost inside MVD barrel
1	95.75°	4.7	noisy
2	28.25°	4.4	good
3	320.75°	3.0	power low
4	275.75°	3.7	OK
5	208.25°	-	not installed

Table 3

Mean and standard deviation, in microns, for the average of ON and OFF residuals for beam-2 at planes 2, 3, 5 and 6 and their differences in the local and global coordinate systems.

LOCAL	P2- <i>y</i>	P3- <i>y</i>	P5- <i>y</i>	P6- <i>y</i>	P2- <i>x</i>	P3- <i>x</i>	P5- <i>x</i>	P6- <i>x</i>
ON	-306.2	-76.4	-253.9	173.2	125.8	35.7	221.1	467.7
	3.9	3.9	4.1	7.4	2.5	5.3	8.8	5.9
OFF	-379.2	-195.8	-378.0	99.9	132.1	51.8	264.4	469.3
	7.5	6.8	2.2	3.4	2.5	5.4	6.8	3.1
DIFF	73.0	119.4	124.1	73.3	6.3	16.1	43.3	1.7
	8.4	7.9	4.7	8.2	3.5	7.5	11.1	6.6

GLOBAL	P2- <i>y</i>	P3- <i>y</i>	P5- <i>y</i>	P6- <i>y</i>	P2- <i>x</i>	P3- <i>x</i>	P5- <i>x</i>	P6- <i>x</i>
ON	329.3	84.2	328.3	68.8	34.1	4.7	-74.6	-493.9
	3.1	2.4	7.5	4.3	3.5	6.1	6.2	8.5
OFF	396.7	197.0	458.1	134.1	63.0	47.1	-53.9	-460.5
	5.8	3.9	3.0	3.4	5.3	7.6	6.2	3.1
DIFF	67.4	112.8	129.7	65.3	28.9	42.4	20.7	33.4
	6.6	4.6	8.1	5.4	6.3	9.8	8.8	9.0

Table 4

Mean and standard deviation, in microns, for the average of ON and OFF residuals for beam-4 at planes 2, 3, 5 and 6 and their differences in the local and global coordinate systems.

LOCAL	P2- <i>y</i>	P3- <i>y</i>	P5- <i>y</i>	P6- <i>y</i>	P2- <i>x</i>	P3- <i>x</i>	P5- <i>x</i>	P6- <i>x</i>
ON	271.0	453.7	-153.8	90.7	-232.0	-28.0	-85.3	-14.6
	5.2	6.6	3.6	1.5	2.0	2.7	1.9	7.4
OFF	240.2	421.0	-185.0	107.1	-246.7	-54.6	-109.4	-46.3
	7.0	8.8	7.5	3.0	4.4	5.4	4.7	8.3
DIFF	30.8	32.7	31.2	16.4	14.7	26.6	24.1	31.7
	8.7	11.0	8.3	3.4	4.9	6.1	5.0	11.1

GLOBAL	P2- <i>y</i>	P3- <i>y</i>	P5- <i>y</i>	P6- <i>y</i>	P2- <i>x</i>	P3- <i>x</i>	P5- <i>x</i>	P6- <i>x</i>
ON	292.9	454.2	-144.4	91.8	203.7	-17.6	100.3	5.4
	5.1	6.5	3.7	1.2	2.1	2.9	1.7	7.4
OFF	263.7	424.4	-173.1	111.2	221.4	12.1	127.4	35.3
	7.2	9.1	7.7	2.8	4.1	5.0	4.2	8.4
DIFF	29.1	29.8	28.6	19.5	17.7	29.7	27.1	29.9
	8.8	11.2	8.6	3.0	4.6	5.8	4.6	11.2